Molecular Dynamics Study of the Active Site of Methylamine Dehydrogenase

Gustavo Pierdominici-Sottile,[†] Julián Echave,[‡] and Juliana Palma*[,†]

Centro de Estudios e Investigaciones, Universidad Nacional de Quilmes, Sáenz Peña 180, B1876BXD Bernal, Argentina, and Instituto Nacional de Investigaciones Fisicoquímicas Teóricas y Aplicadas (INIFTA), Universidad Nacional de La Plata, Suc.4 C.C. 16, 1900 La Plata, Argentina

Received: February 2, 2006; In Final Form: March 31, 2006

We have obtained AMBER94 force-field parameters for the TTQ cofactor of the enzyme methylamine dehydrogenase (MADH). This enzyme catalyzes the oxidation of methylamine to produce formaldehyde and ammonia. In the rate-determining step of the catalyzed reaction, a proton is transferred from the methyl group of the substrate to residue Asp76. We used the new parameters to perform molecular dynamics simulations of MADH in order to characterize the dynamics of the active site prior to the proton-transfer step. We found that only one of the oxygen atoms of Asp76 can act as an acceptor of the proton. The other oxygen interacts with Thr122 via a strong hydrogen bond. In contrast, because of the rotation the methyl group of the substrate, the three methyl hydrogen atoms are alternately in position to be transferred. The distance that the proton has to travel presents a broad distribution with a peak between 1.0 and 1.1 Å and reaches values as short as 0.8 Å. The fluctuation of the distance between the donor and the acceptor has the largest frequency component at 50 cm^{-1}, but the spectrum presents a rich structure between 10 and 400 cm^{-1}. The more important peaks appear below 250 cm^{-1}.

I. Introduction

Methylamine dehydrogenase (MADH) is a soluble quinoprotein that catalyses the oxidation of methylamine to formaldehyde and ammonia.[1,2] The structure of MADH corresponds to an L_2H_2 heterotetramer with molecular weights of approximately 15 500 and 46 700 for the light and heavy subunits, respectively. Each of the light subunits contains a quinone cofactor called tryptophan tryptophylquinone, TTQ, which is shown in Figure 1.

The catalytic mechanism of MADH can be divided into reductive and oxidative half-reactions. In the reductive half, the quinone carbon atom C6 of TTQ (see Figure 1) suffers the attack of methylamine to form an aminoquinol species

$$CH_3NH_2 + MADH_{ox}O \rightarrow HCHO + MADH_{red}NH_2 + H^+ \quad (I)$$

Then, in the oxidative half-reaction, two electrons are sequentially transferred to an electron acceptor, restoring MADH to its oxidized quinone form.[3] Reaction I presents an anomalously large kinetic isotopic effect (KIE).[4] In addition, the KIE is nearly temperature-independent, whereas the rate constants are temperature-dependent.[5] In other words, the activation energies for protium and deuterium were found to be approximately the same, even though the rate constants for protium are nearly 17 times larger than those for deuterium.

In the mechanism proposed for reaction I, the process initiates with the attack of methylamine on quinone atom C6 of TTQ. This produces a carbinolamine intermediate that then loses a water molecule, becoming an iminoquinone species. After that, one of the bases of the active site abstracts a proton from the methyl group of the iminoquinone, leading to the reduction of TTQ.[3] The sequence of steps to this point is shown in Figure 2. It has been suggested that the abstraction of the proton is the step that determines the rate of the process and that the unusually large KIE observed is due to the fact that this transfer occurs mainly by tunneling.

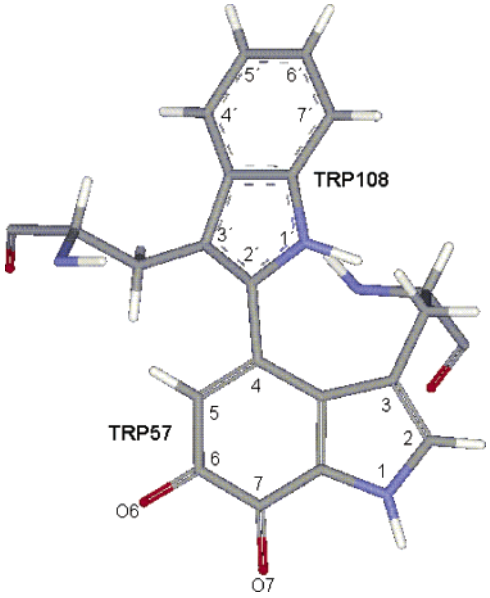

Figure 1. Structure of TTQ in its native form.

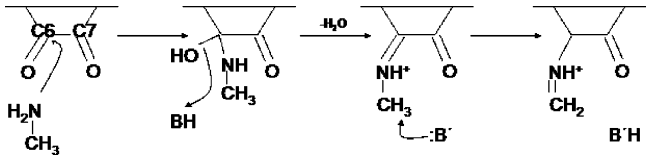

Figure 2. Proposed mechanism for reaction I up to the proton-transfer step.

Several theoretical studies have been performed on reaction I. These studies include transition state theory calculations of

* To whom correspondence should be addressed. E-mail: juliana@unq.edu.ar. Tel.: ++54-11-4365 7100 (ext 135). Fax: ++54-11-4365 7182.
† Universidad Nacional de Quilmes.
‡ Universidad Nacional de La Plata.

10.1021/jp060715+ CCC: $33.50
Published on Web 05/24/2006

the rate constants on an electronically adiabatic surface,[6−9] calculations based on a model in which the process is treated as a coupled proton−electron transfer in the presence of rate-promoting vibrations,[10] calculations based on the golden rule or the instanton approach,[11] and quantum calculations performed on different models of the active site.[12] However, to the best of our knowledge, no molecular dynamics simulations have been performed so far.

Many details of the dynamics of this proton transfer are still unclear. For example, it has been suggested that some vibrations of the protein backbone could enhance H^+-tunneling.[5] However, these vibrations have been neither identified nor characterized. The role of some polar residues of the active site is also unknown. It is believed that they play a role during catalysis.[13] However, their role could not be assessed by site-directed mutagenesis experiments, as it was found that relatively conservative mutations of these residues prevented the protein from achieving a proper folded state.[14] It is interesting to determine the distances that the proton must travel to go from the donor to the acceptor and investigate how these distances are affected by the protonation state of the iminoquinone intermediate.

In this article, we present the results of molecular dynamics simulations of the active site of MADH, prior to the proton-transfer step. To perform this study, we had to derive force-field parameters for the TTQ cofactor. Even though we were mainly interested in the iminoquinone form of TTQ (see Figure 3), as this is the form of the cofactor just before the H^+ transfer, we also derived force-field parameters for TTQ in its native form. In part, this was done for completeness, but more importantly, it was done because many of the parameters used to describe native TTQ can also be used to describe other novel quinone cofactors whose experimental study has received a lot of attention in the past several years.[15,16]

The rest of this article is organized as follows: In section IIa, we describe the main features of the methodology used to obtain the new parameters, and in section IIb, we present and discuss the tests we performed to assess them. The results of the molecular dynamics calculations are presented and discussed in section III. The conclusions of this work are presented in section IV.

II. Parametrization

(a) General Aspects. Here, we briefly describe the general guidelines we followed to obtain the force-field parameters for the TTQ cofactor in the native form and in the protonated and unprotonated iminoquinone forms. A detailed discussion of the procedure can be found in the Supporting Information, along with the keyword parameter files needed to apply the new parameters to a calculation performed with the TINKER package (version 4.0).[17]

The calculations presented in this article were performed using the force-field parameters of AMBER94[18] as implemented in TINKER. To do that, AMBER atom types were assigned to the atoms of the TTQ cofactor using similarity criteria. After this assignment had been performed, we found that the force field did not have parameters to describe several bonds, angles, and torsions. The majority of the corresponding force constants were assigned by similarity as well, or by using the scaling algorithm of Cornell et al.[18] In those cases where neither similarity nor scaling were applicable or where we considered that a more precise description was needed, we derived the force constants by fitting data obtained in quantum mechanical (QM) calculations. The equilibrium values were taken from the corresponding QM-minimized structures. All QM calculations reported in this article were performed with Gaussian 98,[19] using the B3LYP 6-31G(d) level of theory.

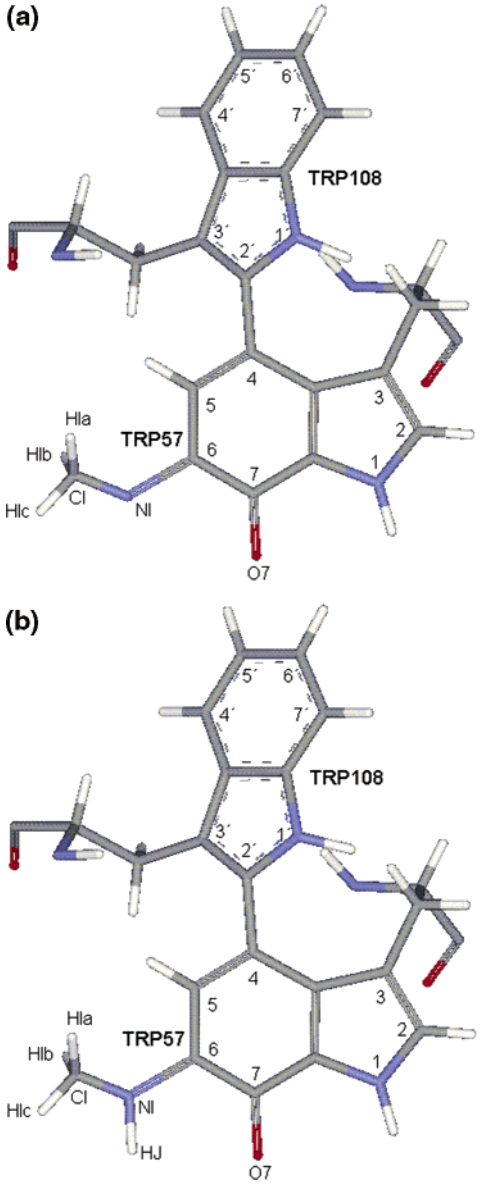

Figure 3. Structure of TTQ in the iminoquinone form: (a) unprotonated, (b) protonated.

The partial charges of the atoms were calculated using the RESP methodology with the standard constraints[20] and using ACE and NME as the blocking groups for the −NH and −CO termini, respectively. The RED program was used to generate the input files for RESP.[21] For the calculations performed on the whole protein, we used the crystal structure of MADH from *Paracoccus denitrificans* resolved at 1.75 Å.[13] This structure was taken from the Protein Data Bank, entry 2BBK. In the following discussion, the numbers of residues correspond to this crystallographic structure.

Table 1 presents all of the parameters that were added to the force field to describe bonded interactions of native TTQ. The parameters corresponding to nonbonded interactions are presented in Table 2. Table 3 lists the parameters added to the force field to describe the bonded interactions of TTQ in the unprotonated iminoquinone form. The parameters corresponding to nonbonded interactions are presented in Table 4. Finally, Table 5 presents the parameters added to describe the nonbonded interactions of TTQ in the protonated iminoquinone form.

TABLE 1: Parameters for Bonded Interactions Added to the AMBER94 Force Field to Describe Native TTQ[a]

bond	K_r[b]	r_{eq}[c]
C−C	310.0	1.570
C−CN	416.0	1.440
CM−CW	357.0	1.480
CM−CB	401.0	1.450
CM−HG	367.0	1.080

angle	Kq[d]	q_{eq}[e]
C*−CB−CM	63.00	134.10
C*−CW−CM	63.00	130.50
CN−CB−CM	63.00	118.80
CB−CN−C	63.00	126.30
CB−CM−CM	63.00	119.20
CB−CM−CW	63.00	121.30
CM−CM−CW	63.00	119.50
C−C−CM	63.00	117.80
C−C−CN	63.00	113.50
C−C−O	80.00	120.00
CN−C−O	80.00	124.10
C−CN−NA	70.00	124.90
CM−CW−NA	70.00	120.40
C−CM−HG	35.00	115.40
CM−CM−HG	35.00	120.50

torsion	$V_n/2$[f]	g[g]	n[h]
X−CB−C*−X	1.675	180.0	2
X−CB−CN−X	3.000	180.0	2
X−CN−NA−X	1.525	180.0	2
X−CM−CM−X	6.650	180.0	2
X−CM−CB−X	1.878	180.0	2
X−C−CM−X	2.175	180.0	2
X−C−CN−X	2.208	180.0	2
X−C−C−X	0.000	−	−
X−CW−C*−X	6.525	180.0	2
X−CW−NA−X	6.525	180.0	2
X−CM−CW−X	0.811	180.0	2
	−0.072	180.0	4
	−0.019	180.0	5

imp torsion	$V_n/2$[f]	g[g]	n[h]
CN−C−C−O	10.50	180.0	2
CM−C−C−O	10.50	180.0	2
NA−C*−CW−CM	1.10	180.0	2
CB−CM−CM−CW	1.10	180.0	2
C−CM−CM−HG	1.10	180.0	2

[a] Atom type HG stands for the hydrogen atom at position 5 of Trp57. X stands for any atom type. The rest of the atoms are labeled according to their AMBER94 types. [b] kcal/(mol Å^2). [c] Å. [d] kcal/(mol rad^2). [e] deg. [f] kcal/mol. [g] Phase offset in deg. [h] Periodicity of the torsion.

(b) Assessment of the New Parameters. As a first test on the quality of the parameters added to the force field, we compared the experimental and minimized structures of subunit L of MADH. The initial structure, taken from the PBD file, was first optimized using a nonlinear conjugate gradient minimization, until the RMS gradient became <0.01 kcal mol^{-1} Å^{-1}. Then, the optimization was completed using a truncated Newton minimization, until the RMS gradient became < 1.0 × 10^{-6} kcal mol^{-1} Å^{-1}. The RMS deviation between the minimized and crystallographic structures for the entire subunit L was 0.9684 Å. When we compared just the positions of the atoms that form the active-site cavity (these are residues 32, 57, 76, 104−108, 119, and 122), the RMSD between the crystal and minimized structures was 0.2720 Å. Thus, the main differences between the calculated and experimental structures were located in residues that are not near the newly parametrized TTQ cofactor. Instead, these differences were observed in residues that are near the surface of subunit L and can be attributed to the lack of interaction with other subunits or with the solvent, which were not included in the minimization.

TABLE 2: Parameters for Nonbonded Interactions Added to the AMBER94 Force Field to Describe Native TTQ[a]

residue Trp57		residue Trp108	
atom	partial charge	atom	partial charge
C	0.5973	C	0.5973
O	−0.5679	O	−0.5679
N	−0.4157	N	−0.4157
HN	0.2719	HN	0.2719
CA	0.0671	CA	−0.0641
HA	0.0615	HA	0.0883
CB	0.0327	CB	0.1754
HB1/HB2	−0.0251	HB1/HB2	0.0034
CG	0.0221	CG	−0.0600
CD1	−0.0460	CD1	0.0325
HD1	0.1363	NE1	−0.3562
NE1	−0.2329	HE1	0.3211
HE1	0.3418	CD2	0.0011
CD2	−0.0493	CE2	0.0873
CE2	−0.0883	CZ2	−0.1452
CZ2	0.4175	HZ2	0.1243
O7	−0.4276	CH2	−0.1468
CH2	0.3741	HH2	0.1282
O6	−0.3988	CZ3	−0.1343
CZ3	−0.0727	HZ3	0.1196
HZ3	0.0417	CE3	−0.0508
CE3	−0.1021	HE3	0.0746

[a] van der Waals parameters: atom type, HG; R^* (Å), 0.9730; e (kcal mol^{-1}), 0.0150. Atom type HG stands for the hydrogen atom at position 5 of Trp57. PDB atom names are used to indicate the partial charges.

TABLE 3: Parameters for Bonded Interactions Added to the AMBER94 Force Field to Describe the TTQ Cofactor in the Unprotonated Iminoquinone Form[a]

bond	K_r[b]	r_{eq}[c]
N2−C	457.0	1.290
CT−HM	340.0	1.090

bending	Kq[d]	q_{eq}[e]
C−C−N2	70.0	114.80
CM−C−N2	70.0	125.90
CT−N2−C	125.57	120.98
HM−CT−HM	35.00	109.50
N2−CT−HM	50.00	109.50

torsion	$V_n/2$[f]	g[g]	n[h]
C−N2−CT−HM	0.000	−	−
X−C−N2−X	10.257	180.0	2
	−2.427	180.0	4
	0.572	180.0	6

imp torsion	$V_n/2$[f]	g[g]	n[h]
CM−C−C−N2	10.50	180.0	2

[a] Atom type HM stands for the hydrogen atoms of the methyl group of the substrate. X stands for any atom type. The rest of the atoms are labeled according to their AMBER94 types. [b] kcal/(mol Å^2). [c] Å. [d] kcal/(mol rad^2). [e] deg. [f] kcal/mol. [g] Phase offset in deg. [h] Periodicity of the torsion.

A second test was performed by comparing the QM- and MM-minimized structures and normal-mode frequencies of the TTQ cofactor. The RMSD between the minimized structures was 0.0916 Å. The angle of torsion between the two indol rings was found to be −48.5° in the QM-minimized structure and −49.0° in the MM-minimized structure. A comparison between the normal-mode frequencies is shown in Figure 4a. Finally, we compared the structures and normal-mode frequencies of TTQ in the iminoquinone form. In this case, the RMSD between

TABLE 4: Parameters for Nonbonded Interactions Added to the AMBER94 Force Field to Describe the TTQ Cofactor in the Unprotonated Iminoquinone Form[a]

residue Trp57		residue Trp108	
atom	partial charge	atom	partial charge
C	0.5973	C	0.5973
O	−0.5679	O	−0.5679
N	−0.4157	N	−0.4157
HN	0.2719	HN	0.2719
CA	0.0678	CA	−0.0527
HA	0.0599	HA	0.0866
CB	0.0742	CB	0.0355
HB1/HB2	−0.0372	HB1/HB2	0.0573
CG	0.0195	CG	−0.0995
CD1	−0.0828	CD1	−0.0506
HD1	0.1432	NE1	−0.3155
NE1	−0.2539	HE1	0.3171
HE1	0.3470	CD2	0.036
CD2	−0.0321	CE2	0.0785
CE2	0.0054	CZ2	−0.1589
CZ2	0.3018	HZ2	0.1245
O7	−0.4364	CH2	−0.1300
CH2	0.4155	HH2	0.1248
NI*	−0.4740	CZ3	−0.1685
CI*	−0.0121	HZ3	0.1250
HIa/HIb/HIc*	0.0606	CE3	−0.0358
CZ3	−0.1966	HE3	0.0725
HZ3	0.2102		
CE3	−0.1388		

[a] van der Waals parameters: atom type, HM; *R** (Å), 0.9789; e (kcal mol^{-1}), 0.0157. Atom type HM stands for the hydrogen atoms of the methyl group of the substrate. PDB atom names are used to indicate the partial charges, except for the atoms denoted with an asterisk (*), which are labeled according to Figure 3a.

TABLE 5: Parameters for Nonbonded Interactions Added to the AMBER94 Force Field to Describe the TTQ Cofactor in the Protonated Iminoquinone Form[a]

residue Trp57		residue Trp108	
atom	partial charge	atom	partial charge
C	0.5973	C	0.5973
O	−0.5679	O	−0.5679
N	−0.4157	N	−0.4157
HN	0.2719	HN	0.2719
CA	0.0181	CA	−0.1304
HA	0.1074	HA	0.1129
CB	0.1610	CB	0.4541
HB1/HB2	−0.0552	HB1/HB2	−0.0553
CG	0.0027	CG	−0.1056
CD1	−0.0531	CD1	0.0327
HD1	0.1669	NE1	−0.2901
NE1	−0.1852	HE1	0.2950
HE1	0.3430	CD2	0.0188
CD2	−0.0500	CE2	0.0887
CE2	−0.0731	CZ2	−0.1483
CZ2	0.4641	HZ2	0.1448
O7	−0.4101	CH2	−0.1025
CH2	0.0168	HH2	0.1475
NI*	−0.1852	CZ3	−0.1248
HJ*	0.2982	HZ3	0.1387
CI*	−0.3417	CE3	−0.0255
HIa/HIb/HIc*	0.1889	HE3	0.0918
CZ3	0.0032		
HZ3	−0.0093		
CE3	0.0116		

[a] van der Waals parameters: atom type, HN; *R** (Å), 0.8467; e (kcal mol^{-1}), 0.0157. Atom type HN stands for the hydrogen atoms of the methyl group of the substrate. PDB atom names are used to indicate the partial charges, except for the atoms denoted with an asterisk (*), which are labeled according to Figure 3b.

the QM- and MM-minimized structures was 0.0689 Å. The equilibrium position for the newly parametrized bending angle C−N2−CT was 122.8° in the QM structure and 122.0° in the MM structure. A comparison between the normal-mode frequencies is shown in Figure 4b.

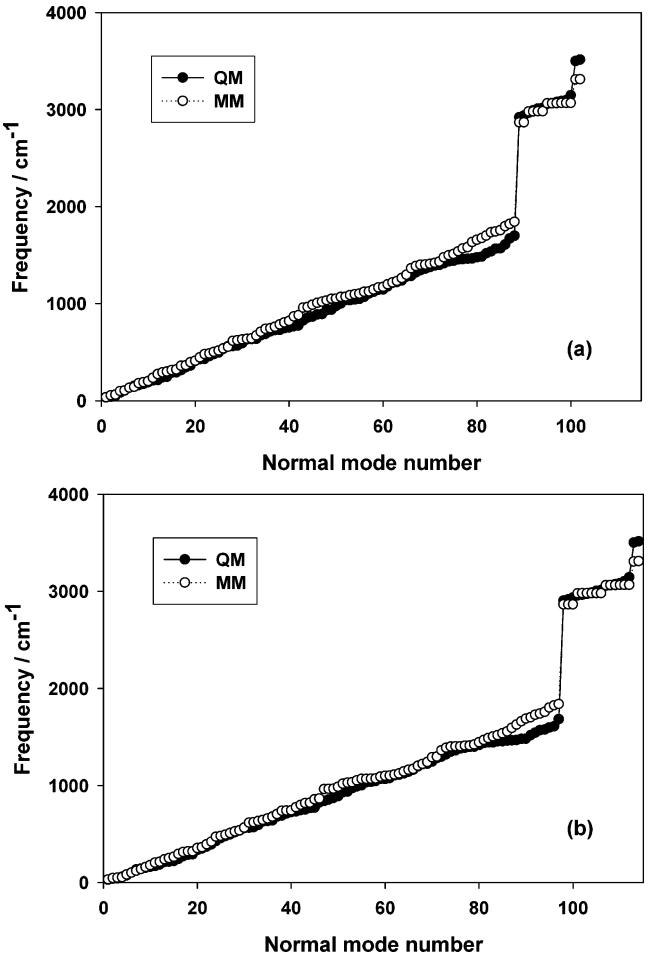

Figure 4. QM and MM normal-mode frequencies: a) native TTQ, (b) iminoquinone form.

Figure 4a,b shows that the larger deviations between the QM and MM frequencies appear in the range between 1200 and 1800 cm^{-1}. Most of the parameters added to the AMBER94 force field have a negligible effect on the vibrations appearing in this range of frequencies. Moreover, differences of the same magnitude are observed if one compares, for example, the QM and MM frequencies of a standard Trp residue, for which all of the force constants are already defined.

III. Molecular Dynamics Simulations

In this section, we present the results of molecular dynamics simulations performed on the light subunit of MADH, with the TTQ cofactor in the iminoquinone form. Both situations, the imino group being protonated and unprotonated, were considered. From the original PDB structure, we took the coordinates of the subunit labeled as L plus the corresponding crystallographic water molecules. Then, we replaced the O6 atom of TTQ with $=N-CH_3$ (or $=NH^+-CH_3$). These groups were oriented so that the $-CH_3$ moiety pointed toward Asp76. There are three water molecules in the active-site cavity. The IDs of their oxygen atoms in the original PDB file are 7731, 7733, and 7740. We removed the molecule corresponding to the atom numbered 7740 to make room to accommodate the $=N-CH_3$ (or $=NH^+-CH_3$) groups. According to the experimental information, this water molecule is weakly bound and can be readily displaced by the substrate.[13] Finally, the system was

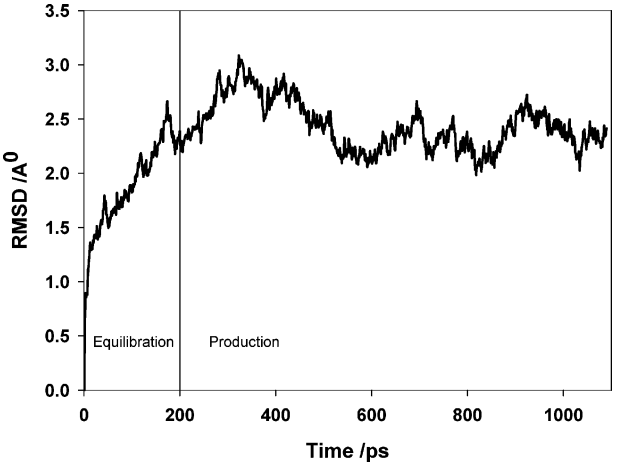

Figure 5. RMSD between the instantaneous and initial structures of subunit L.

TABLE 6: Average Distances between the Hydrogen Atoms of the Methyl Group of the Substrate and the Oxygen Atoms of Asp76

	TTQ form	OD1	OD2
H_a	protonated	3.10	2.87
	unprotonated	3.38	3.03
H_b	protonated	3.10	2.91
	unprotonated	3.38	3.06
H_c	protonated	3.18	2.95
	unprotonated	3.41	3.04

solvated with a rectangular parallelepiped box of water molecules with a distance of 7.0 Å between each wall and the closest atom of the L subunit.

Molecular dynamics simulations were performed using periodic boundary conditions with a cutoff distance of 10.0 Å and a time step of 1.0 fs. The structure generated as explained above was first minimized at constant volume, with a constraint of 500.0 kcal mol^{-1} $Å^{-2}$ on each atom of subunit L. In a second stage, the system was heated from 0 K to a target temperature of 300 K during 35.0 ps using the weak-coupled algorithm with a τ_{tp} value of 2.8 ps. During this heating, the volume was kept constant and a small constraint of 10.0 kcal mol^{-1} $Å^{-2}$ was applied to the atoms of subunit L. After this, we switched to constant-temperature and -pressure conditions, using a value of 2.0 ps for both τ_{tp} and τ_p, so that the density could relax. Configurations sampled every 1.0 ps were used to test the evolution of the temperature, pressure, density, and RMSD, as well as the potential, kinetic, and total energies, until equilibration conditions were attained. This equilibration lasted for 200 ps. Starting with the configuration obtained from the equilibration stage, we performed a dynamic run of 906 ps. During the first 900 ps, configurations were sampled every 1.0 ps. Then, for an interval of 6.0 ps, we sampled configurations every 0.02 ps. In Figure 5, we show the time evolution of the RMSD during the whole dynamic simulation. This was calculated using the initial structure of the equilibration stage as the reference.

With the data sampled from the MD simulation, we calculated the O−H distances between the oxygen atoms of Asp76 and the H atoms of the methyl group of the substrate. In addition, we examined the O−H−C angles, where C is the carbon atom of the methyl group. These parameters are expected to have a large influence on the barrier for H^+ transfer. The average values for the O−H distances are shown in Table 6. The first point that should be noted is that the O−H distances obtained when the imino group is not protonated are always larger than the ones obtained when the group is protonated. This can be attributed to the strong electrostatic interaction that exists between the protonated methylimino group and the carboxylic group of Asp76 and to the fact that R* of the methyl hydrogen atoms is somewhat small in this case (see Tables 4 and 5). Consequently, the transfer of the proton would be favored when the methylimino group is protonated. Thus, from now on, we will concentrate on the dynamics of the active site of MADH for this situation. Nevertheless, the qualitative behavior of the system is similar in both cases.

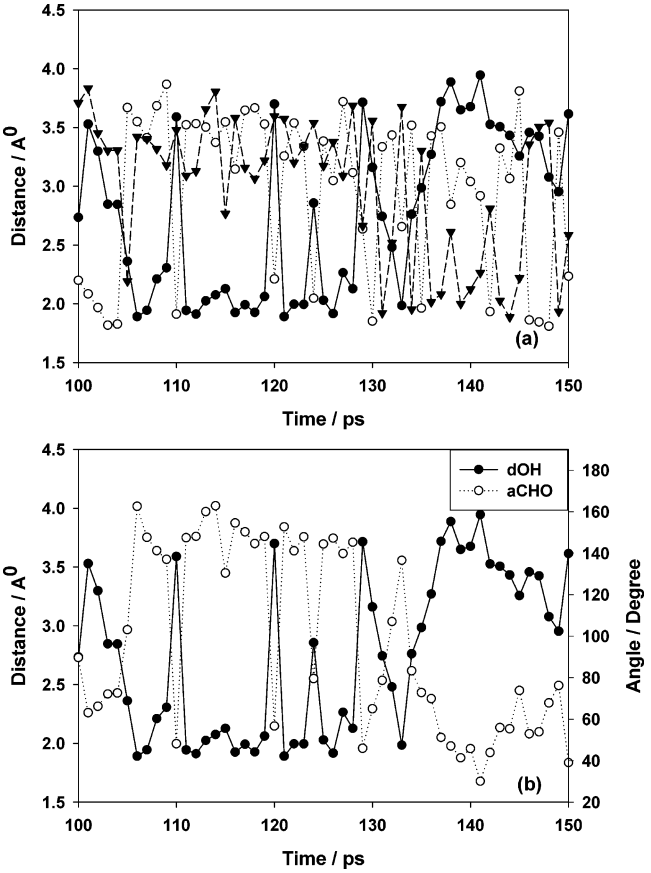

Figure 6. (a) Time evolution of the three O−H distances. The oxygen atom considered is OD2 of Asp76. (b) Co-evolution of an O−H distance with the corresponding O−H−C angle.

Table 6 also shows that the average distances for the three hydrogen atoms are almost the same, whereas the distances that involve atom OD1 of Asp76 are always larger than those that involve atom OD2. This indicates that OD2 is more likely to be the acceptor of the proton than OD1. As a reference, we must say that atom OD1 is the atom that interacts with the side chain of Thr122 whereas atom OD2 interacts with the −NH− group of the peptide bond between Trp108 and Ile107. In this regard, we should note that, in the previous QM study of ref 12, atom OD2 was considered to be the acceptor of the proton, whereas in the studies of refs 6 and 8, the atom equivalent to OD1 was the one considered. We believe that these differences, which can be attributed to the use of different crystalline structures, might have a significant effect on the determination of the height and width of the barrier for proton transfer. Finally, we should note that one of the proposals for reaction I is that the rate-determining step is, in fact, a coupled proton−electron transfer. In that case, the transfer step could be accompanied by a significant structural rearrangement, and the suggestion stated above could cease to be valid.

Figure 6a shows the time evolution of the distances between the hydrogen atoms of the methyl group and atom OD2 of

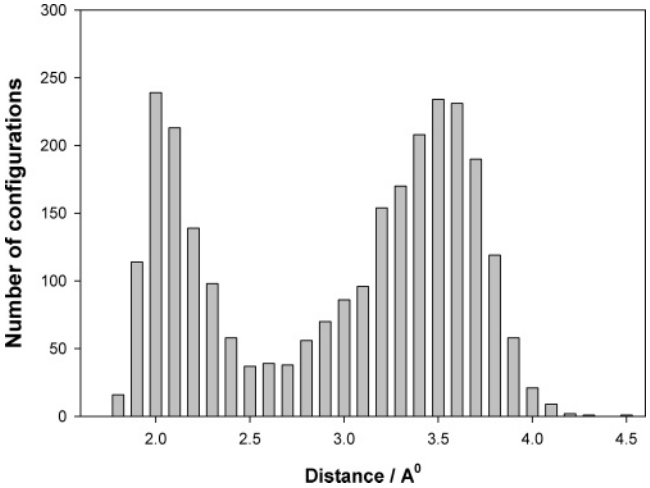

Figure 7. Distribution of the O−H distances observed during the whole dynamic simulation. Labels on the *x* axis indicate the upper limit of each class.

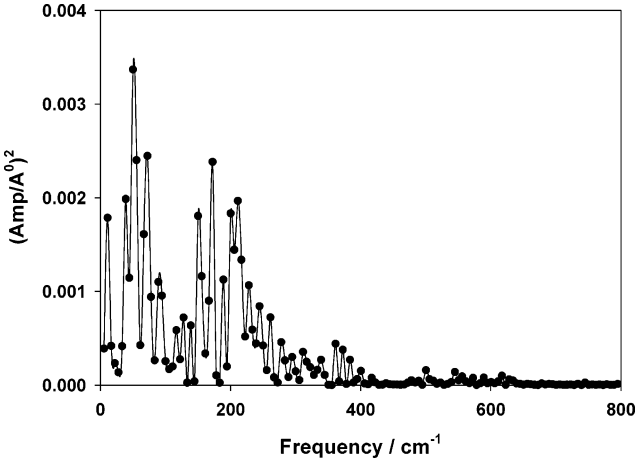

Figure 8. Frequency components of the distance fluctuations between the donor and acceptor of the proton.

Asp76. The data shown in the plots correspond to the interval between 100 and 150 ps of the production phase and are representative of what is observed in the whole dynamic simulation. It can be seen that the three hydrogen atoms are alternately close to atom OD2. Figure 6b shows the co-evolution of one of the O−H distances and the corresponding C−H−O angle. It can be seen that short O−H distances are coincident with large C−H−O angles. Moreover, large changes in the O−H distance are exactly coincident with large changes in the O−H−C angle. This, along with the alternation observed in Figure 6a, indicates that the large changes in the O−H distances are produced by the rotation of the $-CH_3$ moiety about the N−C bond. This rotation explains the fact that the average O−H distances for the three hydrogen atoms are the same. For the same reason, the shortest O−H distances (∼1.7 Å) are significantly smaller than the average O−H distances (∼2.9 Å). Finally, in Figure 7, we show a histogram of the O−H distances of the three hydrogen atoms observed throughout the whole simulation. The distribution presents two peaks, indicating that the most likely distances are 1.9 Å $< d \leq$ 2.0 Å when the H atom is closest to OD2 and 3.4 Å $< d \leq$ 3.5 Å otherwise. It can also be seen that O−H distances near the average value are rather unlikely.

On the other hand, the fact that the average H−OD2 distances are smaller than the H−OD1 distances in the three cases indicates that the carboxyl group of Asp76 does not rotate during the period analyzed. This can be attributed to the strong H-bond interaction between atom OD1 and the −OH group of Thr122. We found that this hydrogen bond is present in 99.0% of the configurations analyzed. This is the highest percentage among all of the H bonds that are present in the initial structure. In this analysis, we considered that a H bond exists when the donor−acceptor distance is smaller than 3.25 Å and the donor−hydrogen-acceptor angle is greater than 150.0°. This suggests that residue Thr122 plays a very important role in the reaction, by fixing the orientation of the carboxylic group so that atom OD2 is in a good position to interact with the methyl group of the substrate.

Siebrand et al.[11] used model calculations to study several enzymatic and nonenzymatic proton-transfer processes in which a C−H bond is broken that present large KIEs with anomalously weak temperature dependences. They suggested that, in all of these systems, a hydrogen bond exists between the donor and the acceptor of the proton. We analyzed the configurations obtained from the molecular dynamics simulations and found that each hydrogen atom of the methyl group is forming an H bond with the OD2 atom of Asp76 in about 11% of the cases. In this analysis, we applied the same criteria as stated above. Thus, when the contributions of the three hydrogen atoms are summed together, it is found that there is an H bond between the methyl group of the substrate and the oxygen atom of Asp76 in one-third of the configurations analyzed. We note, however, that the C−H···O interaction is not strong. If fact, it cannot prevent the rotation of the $-CH_3$ group about the C−N bond. Nevertheless, this analysis must be considered just as a first approach to the subject. A more rigorous treatment would require the use of electronic structure calculations to determine the actual strength of the interaction.

Two parameters that appear in the models used by Siebrand et al. can be estimated from our molecular dynamics simulations. These are the frequency of the promoting vibration and the transfer distance. For the oxidation of methylamine catalyzed by MADH, they found that their model fitted the experimental data using a promoting vibration of 500 cm^{-1} and a transfer distance of 0.5−0.6 Å. The authors pointed out that these values are not reasonable and therefore suggested that there could be some problems with the experimental data. Mincer et al.,[10] on the other hand, used a transfer distance of 0.65 Å and a frequency of 120 cm^{-1} for the promoting vibration in their model.

We performed a fast Fourier transform of the time evolution of the donor−acceptor distance in order to estimate the actual frequency of this rate-promoting vibration. In this analysis, we used the data obtained during the 6-ps interval in which samples were taken every 0.02 ps. Therefore, the maximum frequency component that could be detected was 833.9 cm^{-1}, and the gap between frequency points was 5.6 cm^{-1}. The frequency components determined in this way are shown in Figure 8. It was found that the largest contribution appears at about 50 cm^{-1} and that there are many significant peaks in the range between 10 and 400 cm^{-1}. The most important peaks appear below 250 cm^{-1}. There are also a few rather small peaks at frequencies as high as 600 cm^{-1}. From the simple analysis presented here, we cannot establish the strength or the symmetry of the coupling between each of these vibrations and the reaction coordinate. However, it is important to note that there are significant peaks near 120 cm^{-1} (more exactly, at 90 and 150 cm^{-1}), which is the frequency used in the calculations of Mincer and Schwartz for the promoting vibration symmetrically coupled to the reaction coordinate. On the other hand, the existence of peaks

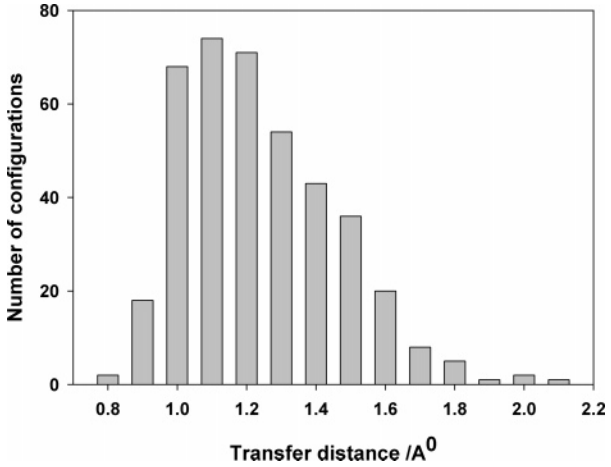

Figure 9. Distribution of transfer distances. Labels on the *x* axis indicate the upper limit of each class.

at relatively high frequencies is consistent with the suggestion of Siebrand and Smedarchina, who postulated that the hydrogen bond between the donor and the acceptor of the proton reduces the donor−acceptor distance and therefore increases the frequency of the corresponding vibration. Finally, we should note that the frequencies presented here correspond to the reactant configuration and therefore are different than the frequencies found at the transition state. However, using previous quantum PM3 calculations performed on models of the active site,[12] we found that, in most cases, there is a one-to-one correspondence between the normal modes of the reactants and those of the transition state and the differences in the corresponding frequencies are normally below 20 cm^{-1}.

To estimate the transfer distances, we proceeded as follows: For each configuration, we found the hydrogen atom nearest to atom OD2 of Asp76. Then, we determined whether, upon moving the H atom away from the C atom, along the direction of the C−H bond, an O−H distance of ≤1.0 Å could be attained. If so, the distance that the H atom had to travel to attain an O−H distance of 1.0 Å was considered to be the transfer distance. In agreement with the previous analysis, we found that, in only one-third of the configurations analyzed, the stretching of the C−H bond leads to the formation of the O−H bond. The distribution of transfer distances obtained in this way is shown in Figure 9. The maximum in the curve is found for 1.00 Å < d ≤ 1.10 Å. It is also observed that some transfer distances fall in the range 0.70 Å < d ≤ 0.80 Å. A closer look at the data reveals that only two configurations belong to this category and that, in both of these, the transfer distance is very close to 0.80 Å. In summary, short transfer distances (≤0.8 Å) are observed, but these situations are not very frequent. As predicted by Siebrand et al., transfer distances as short as those required by the models applied to MADH were not detected.

IV. Conclusions

We obtained AMBER94 force-field parameters for the TTQ cofactor of the enzyme methylamine dehydrogenase in the native, unprotonated iminoquinone, and protonated iminoquinone forms. Many of the parameters obtained can also be used to model other novel quinone cofactors.

Whenever it was possible, we used scaling or similarity criteria to define the new parameters. In those situations in which these strategies could not be applied or when we thought that a more accurate description was needed, we developed new parameters by fitting quantum data calculated at the B3LYP 6-31G(d) level of theory. Partial charges for the atoms were derived using the RESP methodology. The quality of the new parameters was assessed by comparison between MM calculations and QM calculations or experimental results. It was found that the new parameters closely reproduce the QM structures and frequencies of TTQ in the native and iminoquinone forms. Moreover, the new parameters do not distort the structure of the active site of MADH.

We performed MD calculations to gain some insight into the dynamics of the active site of MADH prior to H^+ transfer. We found that the average distances between the hydrogen nucleus to be transferred and the acceptor atom, when the imino group is protonated, are smaller than the distances found when the imino group is not protonated. Because it is believed that the H^+ transfer occurs by tunneling, this indicates that the transfer should be more likely when the imino group is protonated. Nevertheless, we note that other aspects of the reaction that were not analyzed in this work, such as ΔE of reaction, should also be considered.

We found that, for the 900 ps analyzed, the three H atoms of the methyl group of the substrate are equivalent. This is because of the rotation of the $-CH_3$ group about the C−N bond. On the other hand, we found that the OD2 atom of Asp76 is nearer to the H atoms of the methyl group than OD1. This suggests that OD2 is the acceptor of the proton during the rate-determining step of reaction I. Atom OD1, on the other hand, interacts with the hydroxyl hydrogen atom of Thr122 via a strong H bond that is present in 99.0% of the configurations analyzed.

We found that, in one-third of the configurations analyzed, there is a hydrogen atom in good position to be transferred toward the OD2 atom of Asp76. We estimated the transfer distances and found that they present a broad distribution with a maximum occurring at 1.00 Å < d ≤ 1.10 Å. These transfer distances agree with those predicted by model calculations[11] for other enzymatic and nonenzymatic proton-transfer reactions that present large KIEs with small temperature dependences. However, they are significantly larger than those required to reproduce the experimental data available for the proton-transfer step in MADH. On the other hand, we found that the donor−acceptor distance fluctuates with frequencies between 10 and 400 cm^{-1}, with the main components being below 250 cm^{-1}.

In summary, the results presented in this article provide a first insight into the detailed dynamics of the active-site cavity of MADH prior to H^+ transfer. However, there are many aspects of reaction I that require further clarification. In that regard, we have provided data such as transfer distances and frequencies for the promoting vibration that can be used to model the reaction. We also believe that the new parameters for the TTQ cofactor should contribute to facilitate new studies on this intriguing and interesting system.

Acknowledgment. This work was supported by the University of Quilmes, the ANPCyT, and CONICET. We also thank Dr. Sebastián Fernández-Alberti for the corrections and suggestions made after reading this manuscript and the referees for corrections and suggestions that helped to improve the original manuscript.

Supporting Information Available: Detailed discussion of the procedure and tables showing atom types and classes for atoms of TTQ wild type, atom types and classes for atoms of TTQ in the unprotonated iminoquinone form, and atom types and classes for atoms of TTQ in the protonated iminoquinone

form. This material is available free of charge via the Internet at http://pubs.acs.org.

References and Notes

(1) Debeer, R.; Duine, J. A.; Frank, J.; Large, P. J. *Biochim. Biophys. Acta* **1980**, *622*, 370−374.

(2) Davidson, V. L. In *Principles and Applications of Quinoproteins*; Marcel Dekker: New York, 1993; pp 73−95.

(3) Davidson, V. L.; Jones, L. H. *Biochim. Biophys. Acta* **1992**, *1121*, 104−110.

(4) Brooks, H. B.; Jones, L. H.; Davidson, V. L. *Biochemistry* **1993**, *32*, 2725−2729.

(5) Basran, J.; Sutcliffe, M. J.; Scrutton, N. S. *Biochemistry* **1999**, *38*, 3218−3222.

(6) Tresadern, G.; Wang, H.; Faulder, P. F.; Burton, N. A.; Hillier, I. H. *Mol. Phys.* **2003**, *101*, 2775−2784.

(7) Tresadern, G.; Mcnamara, J. P.; Mohr, M.; Wang, H.; Burton, N. A.; Hillier, I. H. *Chem. Phys. Lett.* **2002**, *358*, 489−494.

(8) Faulder, P. F.; Tresadern, G.; Chohan, K. K.; Scrutton, N. S.; Sutcliffe, M. J.; Hillier, I. H.; Burton, N. A. *J. Am. Chem. Soc.* **2001**, *123*, 8604−8605.

(9) Alhambra, C.; Sanchez, M. L.; Corchado, J. C.; Gao, J.; Truhlar, D. G. *Chem. Phys. Lett.* **2002**, *355*, 388−394.

(10) Mincer, J. S.; Schwartz, S. D. *J. Chem. Phys.* **2004**, *120*, 7755−7760.

(11) Siebrand, W.; Smedarchina, Z. *J. Phys. Chem. B* **2004**, *108*, 4185−4195.

(12) Pierdominici Sottile, G.; Echave, J.; Palma, J. *Int. J. Quantum Chem.* **2005**, *105*, 937−945.

(13) Chen, L. Y.; Doi, N.; Durley, R. C. E.; Chistoserdov, A. Y.; Lidstrom, M. E.; Davidson, V. L.; Mathews, F. S. *J. Mol. Biol.* **1998**, *276*, 131−149.

(14) Sun, D. P.; Jones, L. H.; Mathews, F. S.; Davidson, V. L. *Protein Eng.* **2001**, *14*, 675−681.

(15) Rinaldi, A. C.; Rescigno, A.; Rinaldi, A.; Sanjust, E. *Bioorg. Chem.* **1999**, *27*, 253−288.

(16) Davidson, V. L. *Bioorg. Chem.* **2005**, *33*, 159−170.

(17) Pappu, R. V.; Hart, R. K.; Ponder, J. W. *J. Phys. Chem. B* **1998**, *102*, 9725−9742.

(18) Cornell, W. D.; Cieplak, P.; Bayly, C. I.; Gould, I. R.; Merz, K. M.; Ferguson, D. M.; Spellmeyer, D. C.; Fox, T.; Caldwell, J. W.; Kollman, P. A. *J. Am. Chem. Soc.* **1995**, *117*, 5179−5197.

(19) Frisch, M. J.; Trucks, G. W.; Schlegel, H. B.; Scuceria, G. E.; Robb, M. A.; Cheeseman, J. R.; Zakrzewski, V. G.; Montgomery, J. A., Jr.; Stratmann, R. E.; Burant, J. C.; Dapprich, S.; Millam, J. M.; Daniels, A. D.; Kudin, K. N.; Strain, M. C.; Farkas, O.; Tomasi, J.; Barone, V.; Cossi, M.; Cammi, R.; Mennucci, B.; Pomelli, C.; Adamo, C.; Klifford, C.; Ochterski, J.; Petersson, G. A.; Ayala, P. Y.; Cui, Q.; Morokuma, K.; Malick, D. K.; Rabuck, A. D.; Raghabachari, K.; Foresman, J. B.; Cioslowski, J.; Ortiz, J. B.; Stefanov, B. B.; Liu, G.; Liashenko, A.; Piskorz, P.; Kamaromi, I.; Gompertz, R.; Martin, R. L.; Fox, D. J.; Keithz, T.; Al-laham, M. A.; Peng, C. Y.; Nanayakkara, A.; González, C.; Challacombe, M.; Gil, P. M. W.; Jhonson, B. G.; Chen, W.; Wong, M. W.; Andrés, J. L.; Head-Gordon, M.; Replogle, E. S.; Pople, J. A. *Gaussian 98*, revision A.7; Gaussian, Inc.: Pittsburgh, PA, 1998.

(20) Cieplak, P.; Cornell, W. D.; Bayly, C.; Kollman, P. A. *J. Comput. Chem.* **1995**, *16*, 1357−1377.

(21) Pigache, A.; Cieplak, P.; Dupradeau, F. Y. Automatic and highly reproducible RESP and ESP charge derivation: Application to the development of programs RED and X RED. Presented at the ACS National Meeting.